Research Article

Ahmed A. Tayel*, Nancy A. Elsayes, Mohamed M. Zayed, Mohammed A. Alsieni, Fuad A. Alatawi, Adel I. Alalawy, and Amany M. Diab

Powerful antibacterial nanocomposites from *Corallina officinalis*-mediated nanometals and chitosan nanoparticles against fish-borne pathogens

https://doi.org/10.1515/gps-2023-0042
received March 06, 2023; accepted June 12, 2023

Abstract: The fish-borne zoonotic bacteria may pose a risk to humans; nanobiotechnological techniques could serve as effective solutions for fighting them. The direct phycosynthesis of metals' nanoparticles (NPs), silver (AgNPs), and selenium (SeNPs) using *Corallina officinalis* extract (CoE) was achieved. The construction of nanocomposites (NCs) from phycosynthesized NPs and nano-chitosan (NCht) was also accomplished to evaluate these entire compounds/NCs as antibacterial amalgams against fish-borne bacteria, *Aeromonas hydrophila*, *Pseudomonas aeruginosa*, *Salmonella typhimurium*, and *Staphylococcus aureus*. The entire agents/NCs were characterized and assessed. The structure and interactions of chemicals and NCs were determined using infrared analysis. CoE/AgNPs, CoE/SeNPs, NCht, NCht/CoE/AgNPs, and NCht/CoE/SeNPs had mean particles' diameter of 5.52, 12.46, 59.81, 64.59, and 77.16 nm, respectively, which were confirmed by size studies and electron microscopy. The challenged bacteria were entirely susceptible to the inspected agents, using both qualitative and quantitative assays; *S. aureus* was more resistant, while *A. hydrophila* was the most sensitive strain. The NCs (NCht/CoE/AgNPs and NCht/CoE/SeNPs) have the utmost bactericidal potentialities, respectively; they exceeded the action of ampicillin. The total distortion, disintegration, and lysis of the treated *A. hydrophila* cells were highlighted by scanning imaging within 10 h of exposure. The conjugation of CoE-mediated NPs with NCht produced effective and harmless NCs, valid for applications to remove fish-borne pathogens with biosafe characteristics.

Keywords: antimicrobial action, green synthesis, nanopolymers, phycosynthesis, seaweeds

*** Corresponding author: Ahmed A. Tayel,** Department of Fish Processing and Biotechnology, Faculty of Aquatic and Fisheries Sciences, Kafrelsheikh University, Kafrelsheikh 33516, Egypt,
e-mail: ahmed_tayel@fsh.kfs.edu.eg
Nancy A. Elsayes: Department of Fish Processing and Biotechnology, Faculty of Aquatic and Fisheries Sciences, Kafrelsheikh University, Kafrelsheikh 33516, Egypt
Mohamed M. Zayed, Amany M. Diab: Department of Aquaculture (Aquaculture Microbiology), Faculty of Aquatic and Fisheries Sciences, Kafrelsheikh University, Kafrelsheikh 33516, Egypt
Mohammed A. Alsieni: Department of Clinical Pharmacology, Faculty of Medicine, King Abdulaziz University, Jeddah 21589, Saudi Arabia
Fuad A. Alatawi: Department of Biology, Faculty of Science, University of Tabuk, Tabuk 47512, Saudi Arabia
Adel I. Alalawy: Biochemistry Department, Faculty of Science, University of Tabuk, Tabuk 47512, Saudi Arabia

1 Introduction

Human threatening with fetal diseases, including dysenteries, pneumonia, diphtheria, syphilis, typhoid fever, leprosy, tetanus, etc., are frequently caused by pathogenic bacteria [1]. As microorganisms can develop numerous strategies for evading the antibiotics' action (e.g., emerging drug-resistant strains), the search for unusual alternative antimicrobials became an essential communal priority to explore/develop more effectual, cheaper, bioavailable, biosafe, and biocidal agents [2]. Fish (farmed or wildly cultured) are frequently threatened by numerous microorganisms that cause their fatality and may spread via human ingestion or handling [3]. These fish-borne zoonotic microorganisms are frequently the cause of a variety of infectious illnesses that have been identified following contact with or eating of a variety of fish and seafoods [4]. *Staphylococcus aureus* is the pathogen from these fish-borne zoonoses that causes many human illnesses including skin infection and septic/toxic shock syndromes, whereas *Salmonella typhimurium*, along with *Escherichia coli*, was the key causatives of various lethal diseases, e.g., uremia, acute respiratory distress syndrome, typhoid fever,

and hepatic failures [5]. The resistant strains of *Salmonella* spp. and *E. coli* were formerly detected in many seafoods and fresh fish [6]. Additionally, literature has emphasized the most dangerous bacteria that can be spread through fish, such as *Aeromonas hydrophila*, *Vibrio* spp., *Clostridium botulinum*, *E. coli*, *Salmonella* spp., *Shigella* spp., *S. aureus*, *Klebsiella* spp., *Mycobacterium tuberculosis*, *Streptococcus iniae*, *Yersinia* spp., *Brucella* spp., and *Edwardsiella tarda* [4,7,8].

A. hydrophila is a Gram-negative (G^-) zoonotic bacteria that causes large-scale septicemia outbreaks and significant losses in aquaculture [9]; it can transmit to humans to cause gastroenteritis, bacteremia, and necrotizing fasciitis [8]. With the over-use of antibiotics, *A. hydrophila* can express multiple resistances to various antibiotics [10,11].

The resistant strains of Gram-positive (G^+) *S. aureus* were isolated following numerous food poisoning outbreaks [12], including seafood consumption [13].

Macroalgae (seaweeds) comprise large diversified groups of autotrophs; they inhabit the seashores and depth down of ~30 m in oceans, where sufficient light for their photosynthesis is obtainable [14]. Seaweeds have produced a wide range of unique biochemicals (with varied bioactivities), including the anti-ulcers, antibiotics, anticoagulants, anticancers, antiviral, and laxatives [5]. Various bioactive molecules are produced from macroalgae including halogenated terpenoids and sulfated polysaccharides (e.g., carrageenan, fucoidan, and ulvan) that are solely extracted from seaweeds and have potent antimicrobial, anticancerous, and antiviral bioactivities [15,16]. Green chemistry methods were effectively used to synthesize nanoparticles (NPs) from seaweed extracts and derivatives. The phycosynthesized NPs had a variety of sizes, morphologies, and shapes and were used extensively in various pharmaceutical and environmental applications [17–19].

Corallina officinalis (the edible red seaweed) is commonly found worldwide; the bioactive and sulfated polysaccharides of *C. officinalis* demonstrated particular imperative bioactivities such as antitumor, anticoagulant, antithrombotic, antiherpetic, and antiviral (HIV-1) activities [16]. Additionally, the *C. officinalis* extract (CoE) was effectively employed as a mediator for the biosynthesis of several metal NPs, including gold NPs with potent cytotoxic activity [20] and silver (AgNPs) with antifungal and microbicidal activities [17].

The selenium element (Se) offers a natural, non-metallic, and energetic micronutrient for mammals (daily requirements = 30–300 μg); Se could be regularly consumed in the form of a regular diet or supplements [21]. The Se zero-states of oxidation (e.g., Se^0) are often achieved from their NPs (SeNPs), which have minimal toxicity and estimable bioavailability with regard to the further oxidation states of Se [22]. When compared to other (physical–chemical) synthesis methods, the green (biogenic) fabrications of SeNPs offered a significant advantage for applications in pharmacological, nutritional, and medicinal fields because they produced SeNPs that were very stable, non-aggregated, biosafe, and effective [23]. The non-biogenic approaches habitually involved high temperatures, advanced technologies, low pH, hazardous chemicals, and elevated cost, although the biosynthesized SeNPs showed improved bioavailability, larger functionality/bioactivity, and lowermost toxicity [22,24,25]. The frequently reported antibacterial activities of biogenic SeNPs to include reactive oxygen species (ROS) production, cell penetration, interactions with/deactivation of energetic cell organelles, obstruction of metabolic pathways, and distressing cell membrane synthesis and permeabilities [24,26,27].

The conjugations (compositing) of biologically synthesized SeNPs within covering polysaccharides/biopolymers (e.g., chitosan, curcumin, plant mucilage, etc.) were shown to provide SeNPs with more bioactivity and biosafety attributes as powerful antimicrobial conjugates, with lowest biotoxicity potentials [25,28,29].

The biosynthesized silver NPs (AgNPs) were also well confirmed with powerful bactericidal potentialities; the use of biogenic methods for AgNP synthesis significantly reduces biotoxicity toward mammals' tissue while conserving their biocidal activities toward microbes [30,31].

The NPs of biopolymers expressed elevated superiority for applications in drug encapsulating, carrying, or delivery; the nanobiopolymers are potentially excellent in terms of biodegradability, non-toxicity, non-immunogenicity, water solubility, cost-effective, biocompatibility, and self-bioactivity attributes [32,33]. The deacetylated form of chitin, chitosan (Cht), can be obtained from the shells of crustaceans, fungi, plants, or insect skeletons [34]. Cht can be facilely transformed into nanostructures (mostly via ionic cross-linking, self-assembly, or polyelectrolyte development approaches), which generate more effective chitosan NPs (NCht), e.g., the supreme nanocarriers for various drugs/molecules, with _protruding biocompatibilities, biodegradability, negligible immunogenicity, and toxicity [35]. The cationic (positive-charging) nature of Cht and NCht enhanced their desirable adhesion/attachment into anionic (negative-charging) biological surfaces, e.g., cancer cells, microbial surfaces, microbial organelles, DNA, mucosal membranes, and RNA through electrostatic interfaces, which give additional significant rationales to that biopolymer for the delivery and internalization of biomolecules throughout targeted cells/tissues [36].

The term nanocomposite (NC) refers to a conjugation of several materials at the "nano" scale; NCs based on biopolymers usually have a single dimension of less than

1,000 nm [37]. The NCht and additional hydrophilic biopolymer NCs are of outstanding importance for nanobiotechnology applications to deliver therapeutic/bioactive agents, nutraceuticals, genes, antibiotics, anticancer, and assembly of engineered tissues with the highest biosafety qualities [38,39].

The use of CoE-mediated nanomaterials in conjugation with NCht to generate biosafe antimicrobial NCs has not yet been studied.

Accordingly, we focused on using CoE to mediate AgNPs and SeNPs, to create bioactive NCs from the phyco-synthesized NPs with NCht, and to evaluate their prospective antibacterial effects toward fish-borne diseases.

2 Materials and methods

2.1 Chemicals used

Unless otherwise noted, all used chemicals, buffers, media, and reagents were procured from Sigma-Aldrich Co. (St. Louis, MO, USA).

2.2 Algae sampling and processing

The red seaweeds (*C. officinalis*) were hand-harvested off the northern Egyptian coast (near Abu Qir, Alexandria, around 31°18′N, 30°04′E). The morphological recognition of macroalgae specimens was performed by a marine phycologist expert at the National Institute of Oceanography and Fisheries (NIOF; Alexandria, Egypt) and validated to be *C. officinalis* seaweed (Figure 1). The algal samples were thoroughly cleaned/washed with deionized water (DIW), dried (thru warm air at 43 ± 2°C), and pulverized to ~65 mesh size.

2.3 Chitosan extraction

The Cht was extracted from the shell-wastes of *Fenneropenaeus indicus* (white prawn), which was cultivated in an aquaculture research farm at Kafrelsheikh University [40]. The shells were cleaned extensively (manually peeled), dried at 48 ± 2°C, and pulverized. The materials were treated by 20 folds (w/v) of 1.0 N NaOH and then by 1.0 N HCl (for 5 h each at 25 ± 2°C ambient temperature). Each immersing was followed by extensive DIW washing and hot-air drying (45 ± 2°C); then the final powder (chitin) was immersion-treated in 60% NaOH (w/v) solution and autoclaved at 110 ± 2°C for 100 min to de-acetyl chitin and yield Cht. The molecular weight (Mw) of Cht was estimated through gel permeation chromatography (GPC; Water Breeze, Milford, MA, USA), whereas deacetylation degree (DD) was determined from the Cht infrared spectrum using Fourier transform infrared spectroscopy (FTIR; JASCO FTIR-360, Japan).

2.4 Phycosynthesis of metals' NPs

The algal material was immersed in 25 folds (w/v) of DIW and vortexed (240 × *g*) for 4 h at 65 ± 3°C to extract the dried *C. officinalis* powder. The algal residues were omitted through filtration, and the filtered CoE was vacuum evaporated at 43 ± 2°C until dry. While CoE was reconstituted in DIW to get 0.1% (w/v) concentration, fresh suspensions of Na_2SeO_3 and $AgNO_3$ were produced in DIW at 2.0 mM concentration each. For the phycosynthesis of nanometals, 75 mL of each metal suspensions and 25 mL of CoE solution were combined in the dark and vortexed vigorously (730 × *g*) for 125 min without heating [19]. About 2.5 mL of ascorbic acid (1.0% solution) was incorporated into the mixture solution while stirring to prepare SeNPs. When metals are

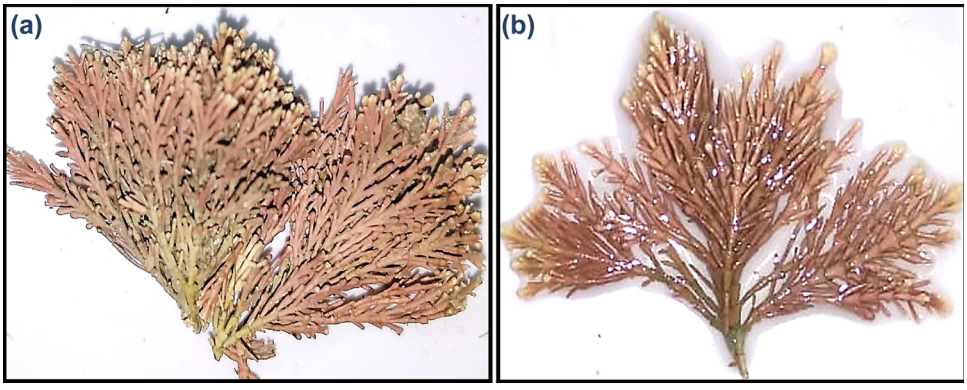

Figure 1: Morphological feature of screened *Corallina officinalis* red algae: (a) dried samples, (b) fresh samples.

reduced to nanoforms, the color of mixed solutions changes from clear to dark brown (for CoE/AgNPs) and brownish-orange (for CoE/SeNPs). The generated NPs were collected by centrifugation (9,400 × *g*, 22 min). For achieving plain AgNPs and SeNPs, the harvested NPs pellets were washed 5 times with DIW and centrifuged after each wash.

2.5 Synthesis of NCht-based nanocomposites

Aqueous acetic acid (1.3%, v/v) solution was created, and 0.1% (w/v) of Cht was thoroughly dissolved in this solution. The pH of this mixture was then changed to 5.5 before filtering. Additionally, a 0.05%, w/v, concentration of Na-tripolyphosphate (TPP) solution in DIW was prepared. The NCht synthesis was directed via dropping (slowly at 18 mL·h^{-1}) of half volume of TPP into the Cht solution, throughout its speedy stirring (710 × *g*), and the stirring continued for 75 min after dropping [41]. The produced NCht was collected by centrifugation (9,100 × *g*, 18 min). For the NCht-based NCs (e.g., NCht/CoE/AgNPs and NCht/CoE/SeNPs), 0.02% (w/v) of CoE/AgNPs and CoE/SeNPs were added into the Cht solution before adding TPP. The mixtures were vortexed for 100 min, then the TPP solution was introduced, and the previous steps were repeated [19]. The designed NPs/NCs were lyophilized and analyzed.

2.6 Nanomaterial characterization

After mixing KBr with samples, the structural and biochemical bonds/groups of CoE, CoE/AgNPs, CoE/SeNPs, NCht, NCht/CoE/AgNPs, and NCht/CoE/SeNPs were examined through FTIR spectroscopy, in transmission mode in the 4,000–450 cm^{-1} range of wavenumber. The spectrophotometry (Shimadzu, UV-2450, Japan) assessed the surface plasmon resonance (SPR) of CoE/AgNPs and CoE/SeNPs, within the wavelength range 200–800 nm. The particle sizes (Ps) and superficial charges (zeta potentiality, ζ) of fabricated NPs/NCs were assessed through a dynamic light scattering (DLS) approach, using Brookhaven zetasizer (ZetaPlus^{TM}, Holtsville, NY, USA). The NPs/NC ultrastructures (e.g., plain AgNPs, SeNPs, CoE/AgNPs, CoE/SeNPs, NCht/CoE/AgNPs, and NCht/CoE/SeNPs) were screened using electron microscopy imaging. The scanning electron microscope (SEM; IT100, JEOL, Tokyo, Japan) and transmission electron microscope (TEM; JEM-100CX, JEOL) were used for screening the Ps, apparent shape, and distributions of nanomaterials.

2.7 *In vitro* antibacterial evaluation

The antibacterial efficacies of CoE, NCht, CoE/AgNPs, CoE/SeNPs, NCht/CoE/AgNPs, and NCht/CoE/SeNPs, in comparison to ampicillin (standard antibiotic, Merck^{TM}; Germany), were evaluated qualitatively/quantitatively against fish-borne pathogens from G^{-} bacteria (*A. hydrophila* – ATCC7966, *P. aeruginosa* – ATCC15692, and *S. typhimurium* – ATCC23852), and G^{+} strains (*S. aureus* – ATCC25923). Nutrient agar/broth (NA/NB, respectively) worked to grow and challenge bacteria under aerobic and warm (37 ± 1°C) conditions. Ampicillin was screened with typical challenges conditions. While the qualitative examination assessed the inhibition zone (ZOI; disc diffusion assay), assessment, the quantitative examination measured the minimum inhibitory concentration (MIC; mg·L^{-1}).

2.7.1 The qualitative examination

The bacterial-inhibition activity was qualitatively evaluated by the ZOI assay. On NA plates, bacterial cultures were swabbed for spreading, and then paper discs impregnated with 0.1% (w/v) of NP/NC solutions were positioned over inoculated plates. After incubation for 22 ± 2 h, the emerged ZOIs (clear zones from grown colonies) were precisely assessed [42].

2.7.2 The quantitative examination

The inhibitory doses from screened NPs/NCs toward challenged pathogens were quantitatively evaluated by the MIC test [42]. The NPs/NCs were diluted successively (from 10 to 100 mg·L^{-1}) and added to NB tubes, which were then injected with bacterial cells (~2 × 10^{6} CFU·mL^{-1}) and allowed to grow for 23 ± 2 h. Then, portions (100 µL) of transparent tubes without noticeable turbidity were injected onto untreated NA plates without nanomaterials and further incubated for an additional cycle. The bacterial-free tubes/plates appointed the nanomaterials MICs toward pathogens.

2.7.3 SEM imagining of NCs bactericidal action

The apparent deformation/distortions in the cellular structure/morphology of *A. hydrophila* were screened following their exposure to NCs (NCht/CoE/AgNPs and NCht/CoE/SeNPs) for 5 and 10 h, compared to control (firstly exposed) cells by SEM imaging. The logarithmic bacterial culture in NB was exposed and incubated with 35.0 and 40.0 µg·mL^{-1}

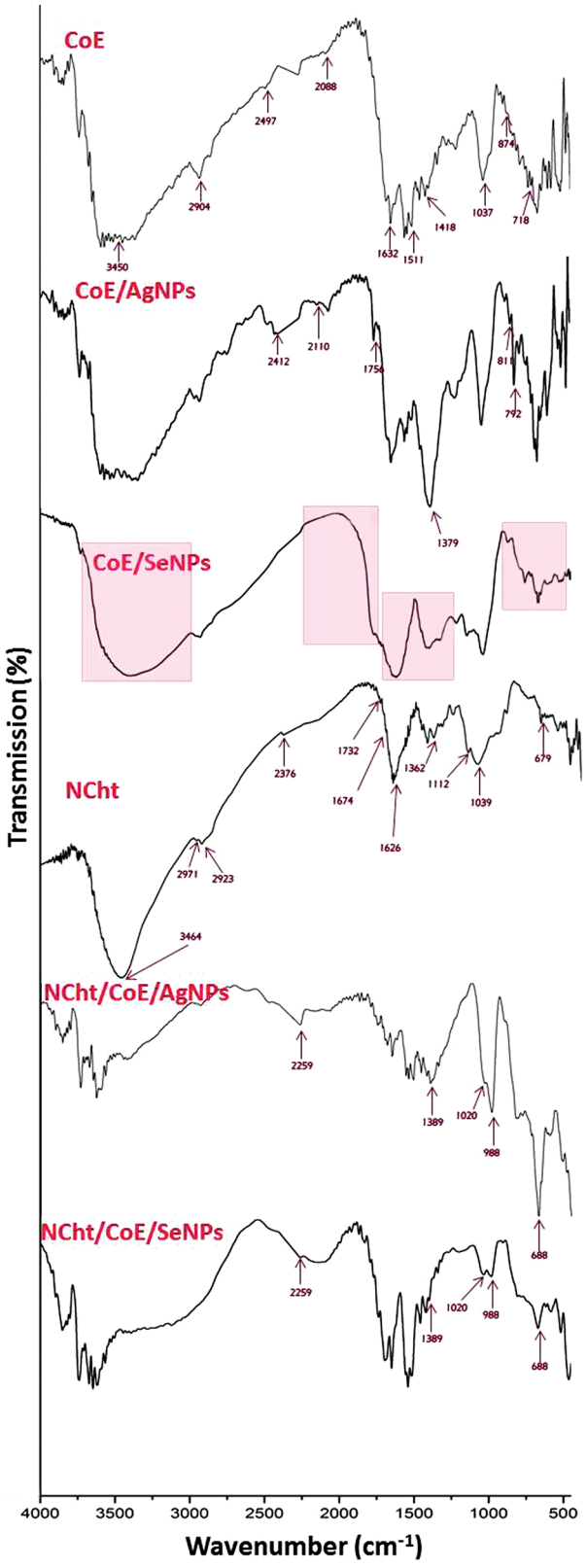

Figure 2: Infra-red spectra of *Corallina officinalis* aqueous extract (CoE), CoE-mediated AgNPs (CoE/AgNPs), CoE-mediated SeNPs (CoE/SeNPs), chitosan nanoparticles (NCht), their combined composites (NCht/CoE/AgNPs and NCht/CoE/SeNPs).

of NCht/CoE/AgNPs and NCht/CoE/SeNPs, respectively. The bacteria were harvested by centrifugation (4,800*g*) after incubation for the required times. The bacteria were then treated for fixation, e.g., with glutaraldehyde 2.5% (30 min), paraformaldehyde 2.0%, and 0.1 M Na-cacodylate buffer (pH 7.25). Successive ethanol concentration treatments dehydrated the cells, which were dried subsequently using Autosamdri-931 (critical-point dryer, Tousimis, Rockville, MD, USA), covered with palladium/gold and imaged with an SEM to check for morphological distortions or changes that had appeared after the cells had been exposed to NCs.

2.8 Statistical analysis

SPSS package (V-21.0, SPSS Inc., Chicago, IL) was used to determine statistical significance at $p \leq 0.05$. ANOVA (one-way) and student *t*-test were used to determine the significant differences from computed triplicates' means.

3 Results and discussion

The Cht was effectively obtained from shrimp wastes, with an Mw of ~158.7 kDa, a DD of ~88.6%, and a yield of 13.6% from the weight of the original shells. It was successful to achieve and characterize the biosynthesis of nanopolymers (e.g., NCht) and nanocomposites (NCs) based on CoE, e.g., CoE-mediated AgNPs (CoE/AgNPs), CoE-mediated SeNPs (CoE/SeNPs), NCht/CoE/AgNPs, and NCht/CoE/SeNPs.

3.1 IR analysis

The FTIR of examined agents/nanocomposites was evaluated to emphasize their key groups/bonds and their potential roles in the synthesis of NPs and interactions between NCs (Figure 2). The FTIR technique is commonly employed to assess NP surface composition, functionalization, and interactions; this method involved the materials' irradiation with infrared waves to record the transmitted or absorbed radiation. The recorded FTIR spectra of compounds could represent unique fingerprints of them, including their nature, polarity, oxidation state, and the involved bonds/groups in their functionalities [18]. In the biosynthesis of metal NPs, the FTIR can highlight the responsible biomolecules and biochemical groups for nanomaterial reduction/stabilization [18].

The IR spectra of CoE revealed the presence of many functional biochemical groups/bonds that were linked to designative constituents of CoE. The main CoE indicative beaks (CoE in Figure 2) were detected at: 1,632.12 cm^{-1} (carboxylic group of uronic acid), 717.91 cm^{-1} (sulfates, the stretched C–S and C═S of sulfides), 874.18 cm^{-1} (bending C–H of glucose and galactose), 1,037.64 cm^{-1} (stretched S═O of starch/polysaccharides sulfonides), 1,418.45 cm^{-1} (stretched C–O and bended O–H of cutin), 1,511.19 cm^{-1} (C═C stretching in lignin), 2,088.36 cm^{-1} (cyanide stretch of nitrile), 2,496.86 cm^{-1} (C–O stretching and P–H stretching of phosphine), 2,904.24 cm^{-1} (stretched CH_3 and CH_2 of aliphatic compounds), and around 3,450 cm^{-1} (stretched O–H of polysaccharides and N–H of amino acids) [5,16,20,43].

The IR spectra of CoE/AgNPs revealed the potential CoE biomolecules that are thought to be responsible for the reduction of Ag^+ ions and the capping of phytosynthesized AgNPs (CoE/AgNPs in Figure 2). In comparison to the plain CoE spectrum, many emerged and more strong bands were appeared in the CoE/AgNP spectrum (e.g., at wavenumbers of 792.54, 811.15, 1,379.44, 1,756.27, 2,109.83, and 2,412.29 cm^{-1}), which indicates the formation of new bonds between the CoE groups and the synthesized AgNPs. Many other peaks were eliminated or became less intense in the CoE/AgNP spectrum (e.g., at wavenumbers of 1,431.25 cm^{-1}), which indicated the presence of these bonds with AgNPs and their interaction with this NM [19,44].

Similarly, the CoE/SeNP spectrum differed from the CoE spectrum in the disappearance of numerous bands in the ranges of 490–920 cm^{-1}, 1,260–1,725 cm^{-1}, 1,770–2,240 cm^{-1}, and at 3,000–3,700 cm^{-1} (highlighted with bale red in CoE/SeNPs in Figure 2), indicating the occupation of such disappeared bonds/groups with SeNPs and their interaction with them during SeNP phycosynthesis and capping [27,29,44].

The cell walls of macroalgae (e.g., *C. officinalis*) frequently contain a variety of functional biomolecules with amine, sulfate, carboxyl, phosphate, and imidazole groups, combined with proteins, alginic acid, and polysaccharides to facilitate interactions, reduce metal ions and cap them during their transformation to nanoforms [17]. Several indicative bands in the CoE spectrum were shifted to close wavelengths, and others appeared with changed intensities after combining with AgNPs and SeNPs, which are assumed to associate with the reduced particles' surface area and their increased crystallinity degrees [18,20,25]. The FTIR spectrum of NCht identified the fundamental bonds/groups that characterize the bulk Cht (NCht in Figure 2) [28]. The key indicative peaks in the plain NCht spectrum included: 3,464.25 cm^{-1} (vibrated N–H and O–H stretching), 2,923.41 cm^{-1} (vibrated aliphatic C–H stretching), 2,970.81 cm^{-1} (vibrated CH_2/CH_3 stretching), 1,732.24 cm^{-1} (stretched C═O of amide I), 1,674.02 cm^{-1} (vibrated stretching of N–H in amide II), 1,112.43 cm^{-1} (–OH vibrated stretching of C3), and 1,038.88 cm^{-1} (–OH vibrated stretching of C6) [41,45]. Furthermore, in the NCht spectrum, the 3,464.25 cm^{-1} band, which frequently showed lower intensity/wider spacing than bulk Cht, provides evidence for reduced –H bonding caused by the interactions with TPP cross-linkage [40]. The existed sharp peak (1,626.32 cm^{-1}) is indicative to cross-linkage between the NH_4 of NCht and TPP [46,47].

The interactions and conjugation between NCht and CoE-mediated NPs (e.g., NCht/CoE/AgNPs and NCht/CoE/SeNPs) resulted in the appearance of the main distinctive peaks from both interacting molecules (NCht/CoE/AgNPs and NCht/CoE/SeNPs in Figure 2), which could convincingly indicate that the occurred interactions among these molecules were physical rather than biochemical associations [19]. Additionally, many distinctive bands in the NCht spectrum were shifted after coupling with both CoE/AgNPs and CoE/SeNPs, e.g., from 2,376.43, 1,361.82, and 112.43 cm^{-1} (–OH vibrated stretching of C3), 1,038.88 cm^{-1} (–OH vibrated stretching of C6), and 679.33 to ~2,259 cm^{-1}, 1,389.44, 1,020, 988, and 688 cm^{-1}, respectively. These shifts could suggest the biochemical interactions between NCht functional groups/bonds and the CoE-mediated nanometals, rather than their physical couplings [32,39,44].

3.2 Optical inspection of phycosynthesized nanometals

The phycosyntheses of CoE-mediated NPs (CoE/AgNPs and CoE/SeNPs) were validated via visual inspection and UV/Vis spectral analysis (Figure 3). The clear suspensions of $AgNO_3$ and Na_2SeO_3 turned dark brown and brownish orange, respectively, after mixing with CoE and reducing metal ions to AgNPs and SeNPs (upper photo in Figure 3). The UV/Vis spectrum of CoE/AgNPs emphasized a distinctive peak at 437 nm, whereas the main maximum absorbance peaks for CoE/SeNPs were recorded at 275 and 211 nm (lower curves in Figure 3). The UV/Vis spectroscopy provides simple and direct indications of NPs' optical properties; the electrons' transition from ground states to excited (nano) states is measured using absorption UV/Vis spectroscopy, which give evidences for nanometals' reduction [18]. The absorbance curve and maximum absorbance value (λ_{max}) of a metal NPs SPR indicate the particle reduction, size distribution, and homogeneity [18,25,29].

The developed brown color and the maximum UV absorbance band at 437 nm are both attributed to SPR of CoE-mediated AgNPs, and validated the effectual biosynthesis of AgNPs after reduction with CoE [33].

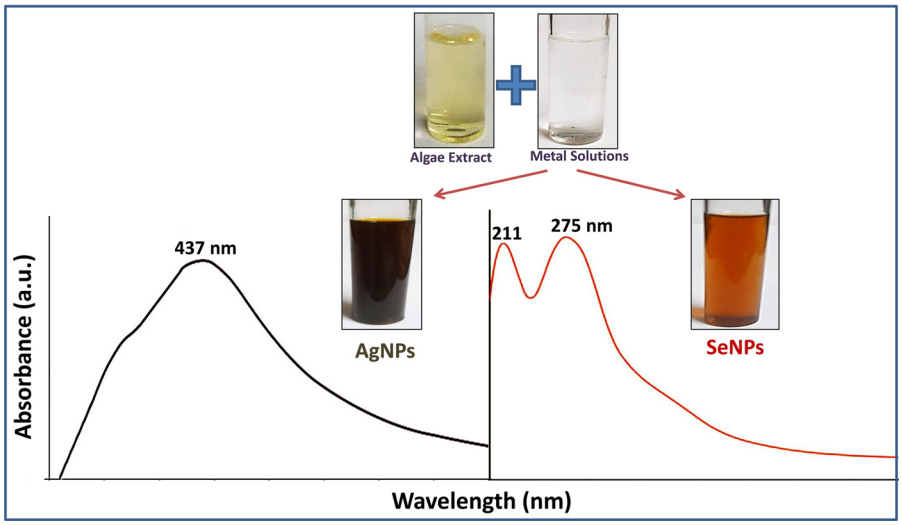

Figure 3: The visual appearance and UV-Vis spectra of *Corallina officinalis* extract-mediated nanometals (AgNPs and SeNPs).

The AgNPs usually have liberated electrons, with vibrated SPR at maximum adsorption at 435–440 nm, which is the distinctive absorption for AgNPs [48,49]. The appearance of a single peak in the CoE/AgNP spectrum could confirm the purity and sole synthesis of the AgNPs [50].

The CoE could immediately transform the Ag solution to brown color (e.g., AgNP formation), indicating the high reducing effectiveness of the extract [51]. As the position and width of the SPR band could indicate particles' shape, charge, size, and interaction with the surrounding medium, the recorded broad band of CoE/AgNPs could indicate the wide distribution of the formed AgNP sizes [52].

The biosynthesis of SeNPs with CoE could be optically proved from the color transformation into brownish orange and the detection of maximum UV absorption peaks at 211 and 275 nm, due to illustrated SPR for SeNPs [53], which confirms the effectiveness of CoE to reduce the Se ions into their NPs form. The less intense peak at 211 nm is usually attributed to a smaller SeNP size [27,53]. The appearance of two absorption bands in the UV/Vis spectrum of the SeNPs and one band of the AgNP spectrum could indicate the uniformity and homogeneousness of synthesized AgNP sizes after reduction with CoE [50–52], whereas the reduction of SeNPs with generated low levels of NP sizes, which could be assumingly attributed to the combined actions of both CoE and ascorbic acid in reducing the Se to NPs [22–27,52,53].

3.3 Ultrastructure analysis of synthesized NPs

The structural physiognomies of generated NPs/NCs were screened via electron microscopic (TEM and SEM) imaging (Figure 4); the precise size and charges of nanomaterials were further determined using zetasizer and DLS approach (Table 1). Harmonized NP/NC sizes were detected using both microscopic imaging and DLS analysis. The TEM images of plain CoE-mediated AgNPs and SeNPs indicated their homogenous sizes and well-distribution (1A and 1S in Figure 4); the NM were mostly spherical with no apparent aggregations among them. The DLS results for CoE-mediated AgNPs and SeNPs were the particles' size means of 5.52 and 12.46 nm, respectively, and the negative charges (−24.8 and −33.2 mV) on their surfaces (Table 1). The microscopic imaging of NCs illustrating their topographical features (SEM images; 2AC and 2SC in Figure 4) and the TEM imaging appraised their sizes and associations between the biopolymer NCht and correlated NM (3AC and 3SC in Figure 4). The NCht/CoE/AgNPs had a smaller size mean (64.59 nm) than NCht/CoE/SeNPs (77.16 nm) and both of them were larger than the plain NCht mean size (59.81 nm). The NCht had strong positive charges (+38.7 mV), and these charges were slightly lessened after conjugation with CoE/AgNPs and CoE/SeNPs to be +34.3 and +32.1, respectively, which indicates the upholding of NCht molecules to NM, where the abundant surface charges were the NCht positives [19,54]. The embedding of CoE/AgNPs and CoE/SeNPs within NCht particles could be evidenced through their TEM images (3AC and 3SC in Figure 4, respectively), where most of the NM were implanted inside the NCht molecules.

As the accustomed NM could impose some potential toxicities to humans, especially when made by chemical/physical approaches, the biosynthesis of such NM with biomolecules (e.g., CoE in this study) could improve their biosafety and biocompatibility [55].

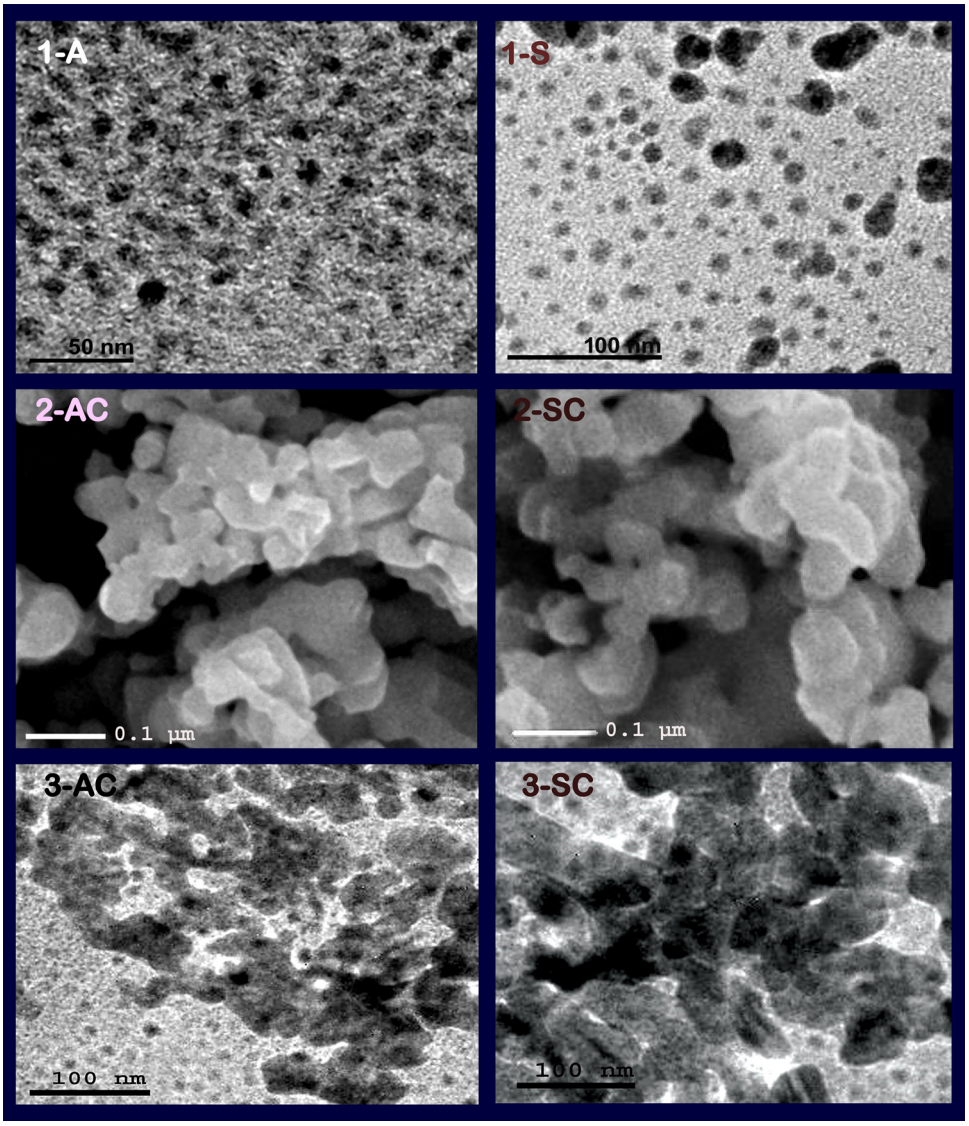

Figure 4: Electron microscopy imaging of synthesized nanomaterials/nanocomposites, including TEM images of plain AgNPs (1-A) and SeNPs (1-S), the SEM imaging of NCht/CoE/AgNPs (2-AC) and NCht/CoE/SeNPs (2-SC) nanocomposites, and the TEM images of the nanocomposites (3-AC and 3-SC, respectively).

Table 1: Particle size distributions and zeta potential of synthesized nanomaterials/nanocomposites

Nanomaterials*	Particle size range (nm)	Mean size diameter (nm)	Zeta potential (mV)
CoE/SeNPs	3.21–31.63	12.46	−33.2
CoE/AgNP	1.34–14.76	5.52	−24.8
NCht	21.92–93.41	59.81	+38.7
NCht/CoE/SeNPs	26.81–112.74	77.16	+32.1
NCht/CoE/AgNPs	24.65–109.66	64.59	+34.3

*CoE/SeNPs: *Corallina officinalis* extract-mediated selenium nanoparticles; CoE/AgNPs: *Corallina officinalis* extract-mediated silver nanoparticles; NCht: nanochitosan.

The CoE/AgNP and CoE/SeNP amalgamations with NCht biopolymer are additionally believed to expressively enhance the NM stabilization, biocompatibility, and bioactivities via the formation of extra functional bonds with the nanopolymer, which can substantially reduce their likely human cytotoxicity [33,56,57].

3.4 Antibacterial assessment

The antibacterial potentialities, emerged after challenging pathogenic strains with screened molecules/NPs/NCs, were proved using qualitative/quantitative assays (e.g., ZOI and

MIC, respectively) (Table 2). The entire compounds/NPs/NCs, e.g., CoE, CoE/SeNPs, CoE/AgNPs, NCht, NCht/CoE/SeNPs, and NCht/CoE/AgNPs, exhibited significant antibacterial powers toward all strains in this order: CoE < NCht < CoE/SeNPs < CoE/AgNP < NCht/CoE/SeNPs < NCht/CoE/AgNPs. The challenged bacteria were entirely susceptible to the inspected agents; their sensitivities to the studied antimicrobials can be arranged in this order: $G^+ < G^-$ (e.g., *S. aureus* < *S. typhimurium* < *P. aeruginosa* < *A. hydrophila*). While many investigated agents exhibited equivalent antibacterial activities to ampicillin, some formulations (especially the NCs) could significantly exceed the bactericidal effect of the standard antibiotic. These results were consistent with earlier studies that used NCht-based NCs for the bacterial challenge [28,40].

The higher resistance of G^+ bacteria to microbicidal nanometals was assumingly attributed to their thick peptidoglycan protective layer, comprising teichoic and lipoteichoic acids, which give G^+ bacteria more barriers to resist NP penetrations into interior cells [40,53]. In contrast, the G^- bacterial cells have thinner peptidoglycan protective layers, less cross-linkage/condensed membranes, and comprise more lipopolysaccharides with high negative charges in the exterior membranes, which lead to the formation of porin channels and increase the penetration of biocidal NPs/NCs into interior cells/vital organelles [58–61].

The porine channels in G^- bacteria could selectively pass penetration of NPs/NM into cells, associating with ROS generation from AgNPs and SeNPs, which lead to the destruction/inactivation of G^- vital components (DNA, proteins, enzymes, etc.) [24,53].

The synergistic bactericidal activities of conjugated NCs (e.g., NCht/CoE/AgNPs and NCht/CoE/SeNPs in this study) were formerly attributed to NCht (highly positive charging) capability for upholding NM, attaching the negative bacterial membranes and increasing their permeability, and its potentialities for inhibiting bacterial biosystems [16,45,62]. The final positive surfaces of the NCs facilitate their attachment with negatively charged bacterial walls and vital components [63]. The biosynthesized NM (AgNPs and SeNPs) were documented to possess powerful bactericidal action, which is chiefly dependent on ROS production and cytotoxicity toward bacterial cells via interaction/inactivation of metabolic pathways [27,55,60]. The conjugation of these NM with biopolymer systems could greatly diminish their toxicity toward mammal tissues but favorably preserve their bioactivities against microbes [55–57].

3.5 Structural analysis of treated bacteria with nanocomposites

For the possible explanation of NCs' (NCht/CoE/AgNPs and NCht/CoE/SeNPs) antibacterial actions, scanning microscopy visualizations were conducted for exposed *A. hydrophila* cells (as the most sensitive strain in antimicrobial assessment) to NCs after 5 and 10 h, compared with zero-time treatments (Figure 5). In zero-time treatment, the bacterial cells appeared with wholesome, smooth, and ordinary structures, with minimum evidence for deformation or distortions or lysis (Se-0 and Ag-0 in Figure 5). After being exposed to NCs for 5 h, numerous deformation/lysis signs were observable on the bacterial surfaces, and many NC particles were seen attached to them. The deformation signs were more

Table 2: Antibacterial potentialities of *Corallina officinalis* extract-mediated nanometals and their composites with nanochitosan against fish-borne pathogens

Antibacterial agent****	Antibacterial activity***							
	Staphylococcus aureus		*Pseudomonas aeruginosa*		*Aeromonas hydrophila*		*Salmonella typhimurium*	
	ZOI*	MIC**	ZOI	MIC	ZOI	MIC	ZOI	MIC
CoE	9.2 ± 0.6$^{\#}$	>100	9.7 ± 0.9$^{\#}$	92.5	9.8 ± 0.8$^{\#}$	85.0	9.5 ± 0.7$^{\#}$	>100
CoE/SeNPs	15.6 ± 1.2$^{\wedge}$	57.5	17.7 ± 1.6$^{\#}$	47.5	17.9 ± 1.8$^{\#}$	45.0	16.4 ± 1.5$^{\#}$	57.5
CoE/AgNPs	17.2 ± 1.5$^{\wedge}$	52.5	21.8 ± 1.9$^{\wedge}$	45.0	22.4 ± 2.3$^{\#}$	42.5	19.6 ± 1.9$^{\wedge}$	50.0
NCht	13.5 ± 0.8$^{\#}$	72.5	16.1 ± 1.5$^{\#}$	62.5	16.8 ± 1.7$^{\#}$	60.0	14.8 ± 1.5$^{\#}$	67.5
NCht/CoE/SeNPs	17.8 ± 1.9$^{\wedge}$	47.5	27.9 ± 2.6$^{\#}$	42.5	28.8 ± 2.6$^{\wedge}$	40.0	23.5 ± 2.1$^{\wedge}$	42.5
NCht/CoE/AgNPs	19.2 ± 2.1$^{\wedge}$	42.5	30.3 ± 2.8$^{\#}$	37.5	32.9 ± 2.9$^{\wedge}$	35.0	26.8 ± 2.7$^{\wedge}$	40.0
Ampicillin	17.5 ± 1.7$^{\wedge}$	52.5	22.7 ± 2.2$^{\wedge}$	40.0	29.8 ± 1.4$^{\wedge}$	40.0	22.1 ± 1.4$^{\wedge}$	45.0

*Zone of inhibition (mm); calculated from triplicates mean ± SD, counting the disc diameter of 6 mm; **MIC – minimal inhibitory concentration, $\mu g \cdot mL^{-1}$; ***Dissimilar symbols (superscript) in one column indicate significant difference ($p \leq 0.05$), compared to standard antibiotic; ****CoE: *Corallina officinalis* extract; CoE/SeNPs: *Corallina officinalis* extract-mediated selenium nanoparticles; CoE/AgNPs: *Corallina officinalis* extract-mediated silver nanoparticles; NCht: nanochitosan.

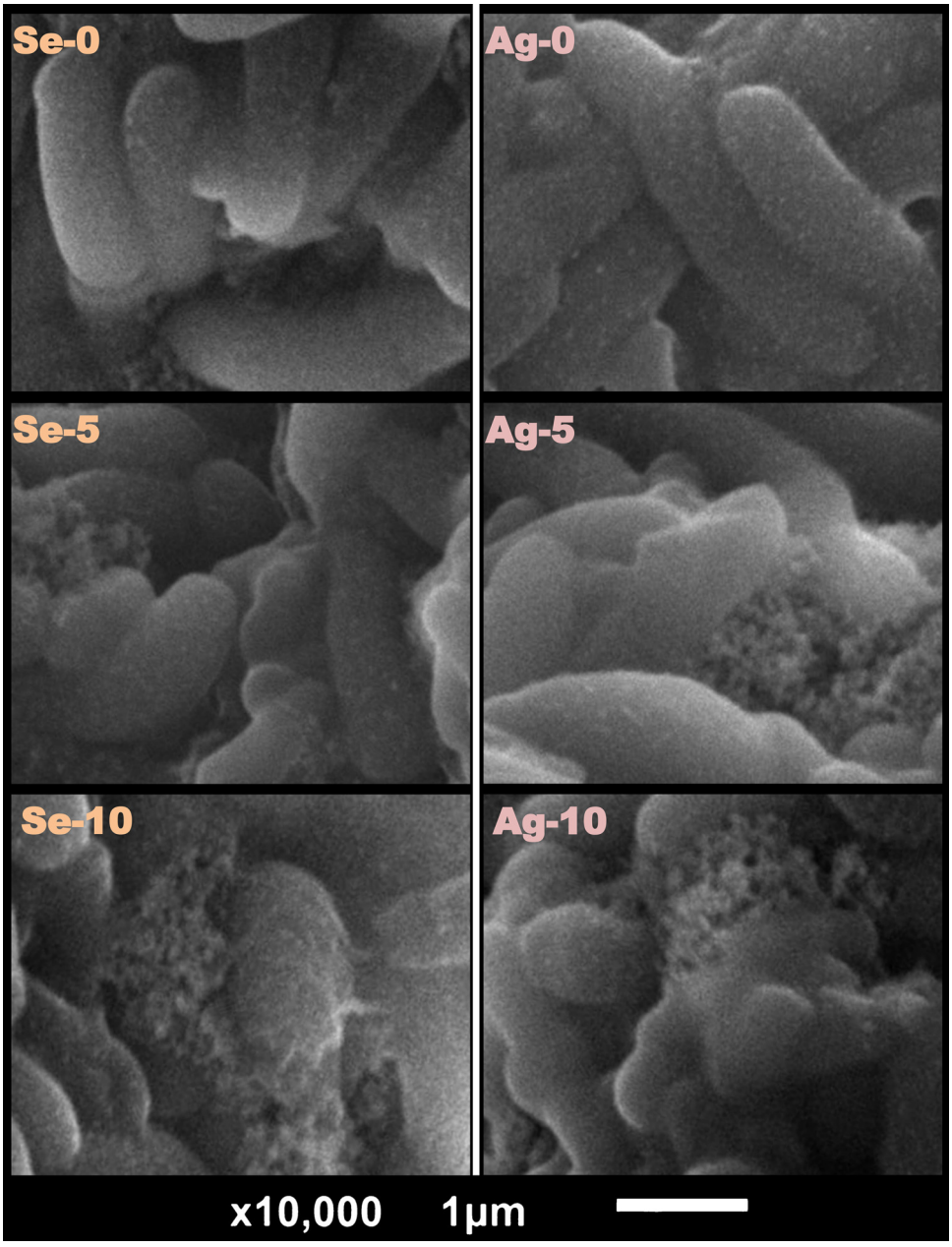

Figure 5: Scanning microscope imaging of exposed *Aeromonas hydrophila* to nanochitosan and *Corallina officinalis* extract-mediated nanometals (Ag and Se) after 0, 5 and 10 h of exposure (the used concentrations from the nanocomposites were 40.0 and 35.0 µg·mL^{-1}, for the Se- and Ag-based composites, respectively).

observable in NCht/CoE/AgNP-treated cells (Ag-5 in Figure 5) than in NCht/CoE/SeNP treatments (Se-5 in Figure 5). After NC exposure for 10 h, most bacterial cells misplaced the uniformed/contacted membranes and liberated their internal constituents (Ag-10 and Se-10 in Figure 5). The NC particles were more observable, interacted with the fully lysed cells and their released internal components. The *A. hydrophila* cells' distortions were also more evidenced with NCht/CoE/AgNP treatments than for NCht/CoE/SeNP exposure. Following treatments of bacteria with NCht-based NCs that contained NM or phyto-constituents, matched observations were reported [33,54].

The role of NCht in the NC antibacterial actions was clear from the captured images, because of its capability to stick onto bacteria, with the accompanied bactericides, and facilitate their movement for penetrating cells [19,62,64].

Since *A. hydrophila* was chosen for the SEM experiment as the most sensitive strain that could provide helpful

explanations and evidence about the NC's actions, the captured images may illustrate that the NCs could have diverse potential mechanisms as antibacterial agents. The probable NCs' effects that originated from the synergism between reacted nanomaterials include the adhesion to cell membranes; increase in membrane permeability; penetration into inner cells; inactivation of cell membrane synthesis; leakages of vital components outside the cells; suppression of the metabolic bioactivities/pathways; and interacting with crucial constituents of cells [24,35].

4 Conclusion

AgNPs and SeNPs were synthesized using CoE as a mediator; the NM had desirable physiognomies, including their minute sizes and synthesis with a diminished toxicity approach. Furthermore, the conjugation between each CoE/AgNP and CoE/SeNP and NCht was conducted and characterized to confirm nanomolecule interaction and compositing to minimize their likely toxicity for humans. The synthetic NCs could effectively inhibit various fish-borne bacterial pathogens with comparable activities to the accustomed antibiotic. SEM imaging was used to validate the antibacterial tests and showed that NCs were acting firmly against harmful microorganisms. The eco-friendly method for NM phycosynthesis and conjugation with nano-biopolymer NCht produced effective and harmless NCs, suitable for use in applications to remove fish-borne pathogens with biosafe characteristics.

Funding information: The authors state no funding involved.

Author contributions: Ahmed A. Tayel contributed in the conception, investigation, interpretation of data, supervision, work drafting and submission; Nancy A. Elsayes contributed in the conception, design of the work, investigation, analysis, and work drafting; Mohamed M. Zayed contributed in design of the work, investigation and analysis, work drafting, supervision; Mohammed A. Alsieni contributed in the formal analysis, interpretation of data, resources, and work drafting; Fuad A. Alatawi contributed in interpretation of data, resources, administration and work drafting; Adel I. Alalawy contributed in interpretation of data, resources, and work drafting; Amany M. Diab contributed in the conception, interpretation of data, work drafting, revising and supervision. All authors read and approved the final manuscript.

Conflict of interest: The authors state no conflict of interest.

Data availability statement: All data generated or analyzed during this study are included in this published article.

References

[1] Kim Y, Gu C, Kim HU, Lee SY. Current status of pan-genome analysis for pathogenic bacteria. Curr Opin Biotechnol. 2020;63:54–62. doi: 10.1016/j.copbio.2019.12.001.

[2] Cano A, Ettcheto M, Espina M, López-Machado A, Cajal Y, Rabanal F, et al. State-of-the-art polymeric nanoparticles as promising therapeutic tools against human bacterial infections. J Nanobiotechnol. 2020;18:1–24. doi: 10.1186/s12951-020-00714-2.

[3] Han BA, Kramer AM, Drake JM. Global patterns of zoonotic disease in mammals. Trends Parasitol. 2016;32:565–77. doi: 10.1016/j.pt.2016.04.007.

[4] Gauthier DT. Bacterial zoonoses of fishes: A review and appraisal of evidence for linkages between fish and human infections. Vet J. 2015;203:27–35. doi: 10.1016/j.tvjl.2014.10.028.

[5] Shobier AH, Ismail MM, Hassan SWM. Variation in anti inflammatory, anti arthritic, and antimicrobial activities of different extracts of common Egyptian seaweeds with an emphasis on their phytochemical and heavy metal contents. Biol Trace Elem Res. 2023;201:2071–87. doi: 10.1007/s12011-022-03297-1.

[6] Zhang J, Yang X, Kuang D, Shi X, Xiao W, Zhang J, et al. Prevalence of antimicrobial resistance of non-typhoidal *Salmonella* serovars in retail aquaculture products. Int J Food Microbiol. 2015;210:47–52. doi: 10.1016/j.ijfoodmicro.2015.04.019.

[7] Shamsi S. Seafood-borne parasitic diseases: A "One-Health" approach is needed. Fishes. 2019;4(1):9. doi: 10.3390/fishes4010009.

[8] Ziarati M, Zorriehzahra MJ, Hassantabar F, Mehrabi Z, Dhawan M, Sharun K, et al. Zoonotic diseases of fish and their prevention and control. Vet Q. 2022;42:95–118. doi: 10.1080/01652176.2022.2080298.

[9] Rahman MT, Sobur MA, Islam MS, Ievy S, Hossain MJ, Zowalaty MEE, et al. Zoonotic diseases: Etiology, impact, and control. Microorganisms. 2020;8(9):1405. doi: 10.3390/microorganisms8091405.

[10] Stratev D, Odeyemi OA. Antimicrobial resistance of *Aeromonas hydrophila* isolated from different food sources: A mini-review. J Infect Public Health. 2016;9:535–44. doi: 10.1016/j.jiph.2015.10.006.

[11] Sun Y, Zhao Y, Xu W, Fang R, Wu Q, He H, et al. Taxonomy, virulence determinants and antimicrobial susceptibility of *Aeromonas* spp. isolated from bacteremia in southeastern China. Antimicrob Resist Infect Control. 2021;10:43. doi: 10.1186/s13756-021-00911-0.

[12] Fisher EL, Otto M, Cheung G. Basis of virulence in enterotoxin-mediated staphylococcal food poisoning. Front Microbiol. 2018;9:436. doi: 10.3389/fmicb.2018.00436.

[13] Vaiyapuri M, Joseph TC, Rao BM, Lalitha KV, Prasad MM. Methicillin-resistant *Staphylococcus aureus* in seafood: Prevalence, laboratory detection, clonal nature, and control in seafood chain. J Food Sci. 2019;84:3341–51. doi: 10.1111/1750-3841.14915.

[14] Mine I. Biological interactions during the life history of seaweed-A microscopic review. Kuroshio Sci. 2008;2:35–40.
[15] Smit AJ. Medicinal and pharmaceutical uses of seaweed natural products: A review. J Appl Phycol. 2004;16:245–62. doi: 10.1023/B:JAPH.0000047783.36600.ef.
[16] Yang Y, Liu D, Wu J, Chen Y, Wang S. In vitro antioxidant activities of sulfated polysaccharide fractions extracted from *Corallina officinalis*. Int J Biol Macromol. 2011;49:1031–7. doi: 10.1016/j.ijbiomac.2011.08.026.
[17] El-Badry A, Assawah S, El-Kassas H, Hegab D, Amer D. New remedy to control human skin fungal infections by silver nanoparticles biosynthesized by two marine macro algae. Middle East J Appl Sci. 2019;59:493–511. doi: 10.21608/ejbo.2019.5351.1219.
[18] Joudeh N, Linke D. Nanoparticle classification, physicochemical properties, characterization, and applications: A comprehensive review for biologists. J Nanobiotechnol. 2022;20(1):262. doi: 10.1186/s12951-022-01477-8.
[19] Alsaggaf MS, Tayel AA, Alghuthaymi MA, Moussa SH. Synergistic antimicrobial action of phyco-synthesized silver nanoparticles and nano-fungal chitosan composites against drug resistant bacterial pathogens. Biotechnol Biotechnol Equip. 2020;34:631–9. doi: 10.1080/13102818.2020.1796787.
[20] El-Kassas HY, El-Sheekh MM. Cytotoxic activity of biosynthesized gold nanoparticles with an extract of the red seaweed *Corallina officinalis* on the MCF-7 human breast cancer cell line. Asian Pac J Cancer Prev. 2014;15:4311–7. doi: 10.7314/APJCP.2014.15.10.4311.
[21] Wang H, Zhang J, Yu H. Elemental selenium at nano size possesses lower toxicity without compromising the fundamental effect on selenoenzymes: Comparison with selenomethionine in mice. Free Radic Biol Med. 2007;42:1524–33.
[22] Wadhwani SA, Gorain M, Banerjee P, Shedbalkar UU, Singh R, Kundu GC, et al. Green synthesis of selenium nanoparticles using *Acinetobacter* sp. SW30: optimization, characterization and its anticancer activity in breast cancer cells. J Nanomed. 2017;12:6841–55. doi: 10.2147/IJN.S139212.
[23] Gad HA, Tayel AA, Al-Saggaf MS, Moussa SH, Diab AM. Phyto-fabrication of selenium nanorods using extract of pomegranate rind wastes and their potentialities for inhibiting fish-borne pathogens. Green Process Synth. 2021;10:529–37. doi: 10.1515/gps-2021-0049.
[24] Shehab MM, Elbialy ZI, Tayel AA, Moussa SH, Al-Hawary II. Quality boost and shelf-life prolongation of African catfish fillet using *Lepidium sativum* mucilage extract and selenium nanoparticles. J Food Qual. 2022;2022:9063801. doi: 10.1155/2022/9063801.
[25] Husen A, Siddiqi KS. Plants and microbes assisted selenium nanoparticles: characterization and application. J Nanobiotechnol. 2014;12:28. doi: 10.1186/s12951-014-0028-6.
[26] Elsaied BEF, Diab AM, Tayel AA, Alghuthaymi MA, Moussa SH. Potent antibacterial action of phycosynthesized selenium nanoparticles using *Spirulina platensis* extract. Green Process Synth. 2021;10:49–60. doi: 10.1515/gps-2021-0005.
[27] Alghuthaymi MA, Diab AM, Elzahy AF, Mazrou KE, Tayel AA, Moussa SH. Green biosynthesized selenium nanoparticles by cinnamon extract and their antimicrobial activity and application as edible coatings with nano-chitosan. J Food Qual. 2021;2021:6670709. doi: 10.1155/2021/6670709.
[28] Gad HA, Alshubaily FA, Alsieni MA, Tayel AA, Diab AM. Biosynthesis of nano-curcumin/nano-selenium composite and their potentialities as bactericides against fish-borne pathogens. Green Process Synth. 2022;11:1098–107. doi: 10.1515/gps-2022-0095.
[29] Siddiqi KS, Husen A, Rao RA. A review on biosynthesis of silver nanoparticles and their biocidal properties. J Nanobiotechnol. 2018;16:14. doi: 10.1186/s12951-018-0334-5.
[30] Slavin YN, Asnis J, Hńfeli UO, Bach H. Metal nanoparticles: Understanding the mechanisms behind antibacterial activity. J Nanobiotechnol. 2017;15:65. doi: 10.1186/s12951-017-0308-z.
[31] Li SR, Huo FY, Wang HQ, Wang J, Xu C, Liu B, et al. Recent advances in porous nanomaterials-based drug delivery systems for cancer immunotherapy. J Nanobiotechnol. 2022;20:277. doi: 10.1186/s12951-022-01489-4.
[32] Elnagar SE, Tayel AA, Elguindy NM, Al-saggaf MS, Moussa SH. Innovative biosynthesis of silver nanoparticles using yeast glucan nanopolymer and their potentiality as antibacterial composite. J Basic Microbiol. 2021;61:677–85. doi: 10.1002/jobm.202100195.
[33] Kou S(Gabriel), Peters LM, Mucalo MR. Chitosan: A review of sources and preparation methods. Int J Biol Macromol. 2021;169:85–94. doi: 10.1016/j.ijbiomac.2020.12.005.
[34] El-Sherbiny MM, Elekhtiar RS, El-Hefnawy ME, Mahrous H, Alhayyani S, Al-Goul ST, et al. Fabrication and assessment of potent anticancer nanoconjugates from chitosan nanoparticles, curcumin, and eugenol. Front Bioeng Biotechnol. 2022;10:1030936. doi: 10.3389/fbioe.2022.1030936.
[35] Jesus S, Marques AP, Duarte A, Soares E, Costa JP, Colaço M, et al. Chitosan nanoparticles: Shedding light on immunotoxicity and hemocompatibility. Front Bioeng Biotechnol. 2020;8:100. doi: 10.3389/fbioe.2020.00100.
[36] Bamburowicz-Klimkowska M, Poplawska M, Grudzinski IP. Nanocomposites as biomolecules delivery agents in nanomedicine. J Nanobiotechnol. 2019;17:48. doi: 10.1186/s12951-019-0479-x.
[37] Soppimath KS, Aminabhavi TM, Kulkarni AR. Biodegradable polymeric nanoparticles as drug delivery devices. J Control Release. 2001;70:1–20. doi: 10.1016/S0168-3659(00)00339-4.
[38] Rajam M, Pulavendran S, Rose C, Mandal AB. Chitosan nanoparticles as a dual growth factor delivery system for tissue engineering applications. Int J Pharm. 2011;410:145–52. doi: 10.1016/j.ijpharm.2011.02.065.
[39] Tayel AA, Elzahy AF, Moussa SH, Al-Saggaf MS, Diab AM. Biopreservation of shrimps using composed edible coatings from chitosan nanoparticles and cloves extract. J Food Qual. 2020;2020:8878452. doi: 10.1155/2020/8878452.
[40] Alsharari SF, Tayel AA, Moussa SH. Soil emendation with nano-fungal chitosan for heavy metals biosorption. Int J Biol Macromol. 2018;118:2265–8. doi: 10.1016/j.ijbiomac.2018.07.103.
[41] Tayel AA, El-tras WF, Moussa S, El-baz AF, Mahrous H, Salem MF, et al. Antibacterial action of zinc oxide nanoparticles against foodborne pathogens. J Food Safe. 2011;31:211–8. doi: 10.1111/j.1745-4565.2010.00287.x.
[42] Ismail MM, Amer MS. Characterization and biological properties of sulfated polysaccharides of *Corallina officinalis* and *Pterocladia capillacea*. Middle East J Appl Sci. 2020;34:623–32. doi: 10.1590/0102-33062020abb0121.
[43] AlMasoud N, Alhaik H, Almutairi M, Houjak A, Hazazi K, Alhayek F, et al. Green nanotechnology synthesized silver nanoparticles: Characterization and testing its antibacterial activity. Green Process Synth. 2021;10(1):518–28. doi: 10.1515/gps-2021-0048.
[44] Rajeshkumar S, Tharani M, Rajeswari VD, Alharbi NS, Kadaikunnan S, Khaled JM, et al. Synthesis of greener silver nanoparticle-based chitosan nanocomposites and their potential antimicrobial activity against oral pathogens. Green Process Synth. 2021;10(1):658–65. doi: 10.1515/gps-2021-0060.
[45] El Rabey HA, Almutairi FM, Alalawy AI, Al-Duais MA, Sakran MI, Zidan NS, et al. Augmented control of drug-resistant *Candida* spp.

via fluconazole loading into fungal chitosan nanoparticles. Int J Biol Macromol. 2019;141:511–6. doi: 10.1016/j.ijbiomac.2019.09.036.
[46] Alalawy AI, El Rabey HA, Almutairi FM, Tayel AA, Al-Duais MA, Zidan NS, et al. Effectual anticancer potentiality of loaded bee venom onto fungal chitosan nanoparticles. Int J Polym Sci. 2020;2020:2785304. doi: 10.1155/2020/2785304.
[47] Salem SS, Fouda A. Green synthesis of metallic nanoparticles and their prospective biotechnological applications: An overview. Biol Trace Elem Res. 2020;199:344–70. doi: 10.1007/s12011-020-02138-3.
[48] El-Abd NM, Hamouda RA, Al-Shaikh TM, Abdel-Hamid MS. Influence of biosynthesized silver nanoparticles using red alga *Corallina elongata* on broiler chicks' performance. Green Process Synth. 2022;11(1):238–53. doi: 10.1515/gps-2022-0025.
[49] El-Baz AF, El-Batal AI, Abomosalam FM, Tayel AA, Shetaia YM, Yang ST. Extracellular biosynthesis of anti-*Candida* silver nanoparticles using *Monascus purpureus*. J Basic Microbiol. 2016;56:531–40. doi: 10.1002/jobm.201500503.
[50] Mouzaki M, Maroui I, Mir Y, Lemkhente Z, Attaoui H, El Ouardy K, et al. Green synthesis of silver nanoparticles and their antibacterial activities. Green Green Process Synth. 2022;11(1):1136–47. doi: 10.1515/gps-2022-0061.
[51] Alwhibi MS, Soliman DA, Awad MA, Alangery AB, Al Dehaish H, Alwasel YA. Green synthesis of silver nanoparticles: Characterization and its potential biomedical applications. Green Process Synth. 2021;10:412–20. doi: 10.1515/gps-2021-0039.
[52] Fardsadegh B, Vaghari H, Mohammad-Jafari R, Najian Y, Jafarizadeh-Malmiri H. Biosynthesis, characterization and antimicrobial activities assessment of fabricated selenium nanoparticles using *Pelargonium zonal*e leaf extract. Green Process Synth. 2019;8(1):191–8. doi: 10.1515/gps-2018-0060.
[53] Youssef DM, Alshubaily FA, Tayel AA, Alghuthaymi MA, Al-Saman MA. Application of nanocomposites from bees products and nano-selenium in edible coating for catfish fillets biopreservation. Polymers. 2022;14(12):2378. doi: 10.3390/polym14122378.
[54] Długosz O, Szostak K, Staroń A, Pulit-Prociak J, Banach M. Methods for reducing the toxicity of metal and metal oxide NPs as biomedicine. Materials. 2020;13(2):279. doi: 10.3390/ma13020279.
[55] Saravanakumar G, Jo D-G, H. Park J. Polysaccharide-based nanoparticles: A versatile platform for drug delivery and biomedical imaging. Curr Med Chem. 2012;19:3212–29. doi: 10.2174/092986712800784658.
[56] Zienkiewicz-Strzałka M, Deryło-Marczewska A. Small AgNP in the biopolymer nanocomposite system. Int J Mol Sci. 2020;21(24):9388. doi: 10.3390/ijms21249388.
[57] El Shafey AM. Green synthesis of metal and metal oxide nanoparticles from plant leaf extracts and their applications: A review. Green Process Synth. 2020;9(1):304–9. doi: 10.1515/gps-2020-0031.
[58] Godlewska-żyłkiewicz B, Świsłocka R, Kalinowska M, Golonko A, Świderski G, Arciszewska Ż, et al. Biologically active compounds of plants: Structure-related antioxidant, microbiological and cytotoxic activity of selected carboxylic acids. Materials. 2020;13(19):4454. doi: 10.3390/ma13194454.
[59] Breijyeh Z, Jubeh BKR. Resistance of gram-positive bacteria to current antibacterial agents and overcoming approaches. Molecules. 2020;25(6):1340. doi: 10.3390/molecules25122888.
[60] Bloukh SH, Edis Z, Sara HAAM. Antimicrobial properties of *Lepidium sativum* L. facilitated silver nanoparticles. Pharmaceutics. 2021;13(9):1352. doi: 10.3390/pharmaceutics13091352.
[61] Tayel AA, Ghanem RA, Al-Saggaf MS, Elebeedy D, Abd El Maksoud AI. Application of fish collagen-nanochitosan-henna extract composites for the control of skin pathogens and accelerating wound healing. Int J Polym Sci. 2021;2021:1907914. doi: 10.1155/2021/1907914.
[62] Larsson M, Hill A, Duffy J. Suspensionstability; why particle size, zeta potentialand rheology are important. Ann Trans Nord Rheol Soc. 2012;20:209–14.
[63] Manivasagan P, Oh J. Marine polysaccharide-based nanomaterials as a novel source of nanobiotechnological applications. Int J Biol Macromol. 2016;82:315–27. doi: 10.1016/j.ijbiomac.2015.10.081.
[64] Sarkar J, Mridha D, Davoodbasha MA, Banerjee J, Chanda S, Ray K, et al. A state-of-the-art systemic review on selenium nanoparticles: Mechanisms and factors influencing biogenesis and its potential applications. Biol Trace Elem Res. 2023. doi: 10.1007/s12011-022-03549-0.